Kombinierte Geschwindigkeits- und Temperaturmessungen mittels LED und einer Doppelbildkamera

A combined velocity and temperature measurement with an LED and a double-frame camera

Zhichao Deng, **Jörg König, Christian Cierpka**
Institut für Thermo- und Fluiddynamik, TU Ilmenau, Am Helmholtzring 1, 98683 Ilmenau

Key words: laser-induced heating, microfluidics, astigmatism particle tracking velocimetry, luminescence lifetime imaging

Abstract

In many fluid dynamical problems, additional temperature measurements are necessary to understand the underlying physics. Luminescence lifetime imaging is a common technique that uses the temperature dependent lifetime of particles doped with a temperature sensitive dye. The technique typically requires a powerful laser and high-speed cameras. In the case of microfluidics, where the optical access is limited, luminescence lifetime imaging was combined with astigmatism particles tracking. With this combined measurement technique, the temperature and all velocity components of spherical tracer particles in a volume of fluid can be measured with only one optical access. However, the generally used light-source, namely the high-energetic pulsed laser might cause additional heating when the volume of fluid is small or the fluid is almost stagnant. Here we show that this problem can be solved by replacing the pulsed laser with an LED. Because of the much-reduced power of the light-source, the heating of the fluid is negligible. To compensate for the lower power provided by the LED, we adapted the timing schedule vastly extended the illumination and the exposure time. In addition, we replaced the typically used high-speed camera with an ordinary double-frame camera with a more sensitive sCMOS sensor. With these adaptations, a comparable signal-to-noise ratio was achieved, which guarantees low measurement uncertainties for all measured quantities. With the current setup, considering complex measuring conditions with varying temperature and locations, the uncertainties for the measurement of the lateral locations x and y, the depth location z and the temperature T were around $0.2\ \mu m$, $0.5\ \mu m$ and $1.0°C$, respectively. Compared with the conventional timing schedule, the movement of the tracer particle during the long illumination and exposure time is significantly enlarged, limiting the maximum measurable range of the velocity. However, several advantages are gained, including the the lower cost of hardware devices, the comparable measurement uncertainties, and most important, the circumvention of light-source induced heating.

Introduction

Microfluidic devices and techniques offer various advantages in the field of biological or chemical assays. In many microfluidic devices, temperature changes and fluid flow occur simultaneously in all three spatial dimensions, and both of them are critical for the performance of these devices. An acoustic tweezer using ultrasonic waves to manipulate small objects is one example (Collins et al. 2015). When these objects are located in the acoustic fields, they can

be moved by either the acoustic radiation force or the viscous drag force. However, due to the power imposed on the system by acoustic actuation, the temperature in the system can increase (Das et al. 2019; Deng et al. 2021). The heating may cause irreversible damage to the manipulated objects if they are sensitive to the temperature change (e.g. biological samples). Thus, it is necessary to conduct a combined 3D velocity and temperature measurement on this acoustic tweezer, capturing key features of the acoustic tweezer, including both the acousto-phoretic movement and the acoustothermal heating.

Astigmatism particle tracking velocimetry (APTV) coupled with luminescence lifetime imaging (LLI) (Cierpka et al. 2012; Massing et al. 2018) is especially suitable for this purpose. Using spherical tracer particles dyed with appropriate luminescence dye as objects manipulated by the acoustic tweezer, all three velocity components in a volume together with the temperature of these particles can be simultaneously measured. It avoids averaging and only needs one optical access and one camera, which is especially suitable for the limited optical access when a microscope is used.

As light source, typically a high-energetic pulsed laser is required to ensure a high signal-to-noise ratio of the acquired images, on which low measurement uncertainties are relied. However, when the measurement technique was applied on the aforementioned acoustic tweezer, significant heating was observed even when no other power was applied to the system (Deng et al. 2021). The reason for this is the laser-induced heating. In the acoustic tweezer, the microfluidic chamber has a very tiny volume of $120\,\mathrm{nl}$, and the fluid in the chamber is almost in quiescent state. As a result, the light-source induced heating has to be carefully excluded.

For this purpose, we replaced the pulsed laser with an LED and developed a novel timing schedule to compensate for the reduced power provided by the LED. Additionally, since the particles inside the microfluidic chamber were exposed multiple times, the measurement bias caused by photobleaching was also considered in the calibration approach. With these adaptations, low uncertainties on the measured quantities can be achieved under complex measuring conditions with varying locations and temperatures.

In the following, the adapted measurement setup and timing schedule, the calibration procedure, discussion on the measurement uncertainties, and a demonstrative measurement on the acoustic tweezer will be outlined in detail.

Measurement setup and principle

The measurement setup is depicted in **Figure 1**. A UV-LED with a central wavelength of $365\,\mathrm{nm}$ (Solis365C, Thorlabs Inc.) was used to illuminate temperature sensitive tracer particles made of PMMA and doped with the luminescence dye europiumtheonyltrifluoracetate (EuTTA, ex. $360\,\mathrm{nm}$/em. $614\,\mathrm{nm}$, $10\,\mathrm{\mu m}$, Surflay Nanotec GmbH) (Massing et al. 2016). We observed them through a microscope (Axio Observer 7, Zeiss GmbH) with an objective lens ($20\times/0.4$, Plan-Neofluar, Zeiss GmbH). A long-pass dichroic mirror (86-330, Edmund Optics) with a cut-on wavelength of 409 nm was used to reflect the excitation light and transmit the emission light. An additional long-pass filter (cut on wavelength $550\,\mathrm{nm}$, FELH0550, Thorlabs Inc.) further reduced the excitation light signal. A sequence of double-frame images were recorded by a camera (Imager sCMOS, LaVision GmbH) with a frame rate of $10\,\mathrm{Hz}$. The precise control of the timing schedule of the camera shutter and illumination was realized by a programmable timing unit (PTU X, LaVision GmbH). For the 3D location measurement with APTV, a cylindrical lens with a focal length of $250\,\mathrm{mm}$ was placed in front of the camera sensor, resulting in different scaling factors of $0.384\,\mathrm{\mu m/pixel}$ in the x-direction and $0.326\,\mathrm{\mu m/pixel}$ in the y-direction, respectively. The measurement volume was around $830\times835\times80\,\mathrm{\mu m}^3$. The LiNbO3 substrate is a key component of the acoustic tweezer and it is a birefringent material. Thus, an

additional polarizer was used to block the extraordinary image for the measurement conducted on the acoustic tweezer.

The measurement on the 3D velocity follows the standard approach of APTV. As depicted in the raw image of frame 1 given in **Figure 2 left**, because of the astigmatism generated by the cylindrical lens, the image of a spherical particle has an elliptical shape. Its x- and y-coordinates are determined by the centroid of the particle image X and Y. The z-coordinate can be expressed as a function of the length of the major and minor axes of the ellipse AX and AY (Cierpka et al. 2011; Cierpka et al. 2010). By tracking particles in between two subsequent light pulses (Cierpka et al. 2013), the three-dimensional velocity distribution can be determined.

The main adaptation was applied on the temperature measurement based on LLI. For the standard technique, after a strong photoexcitation of the pulsed laser, the signal strength of the photoluminescence decays exponentially with the time constant (luminescence lifetime τ). The higher the temperature, the faster the decay and the shorter the lifetime τ. As can be seen in the general timing schedule given in **Figure 2 right**, with the laser, by capturing two frames several μs after the photoexcitation, the luminescence lifetime τ of a particle image can be determined from the ratio between its intensities on the two frames $R := I_2/I_1$. Assuming the grayscale of the particle image is Gaussian-distributed, which is shown in the second column in **Figure 2 left**, the amplitude of the 2D Gaussian distribution is used as an indicator of intensity I. Since τ is a function of the temperature T, a bijection exists between T and R. In practice, this one-to-one correspondence is determined by a calibration.

Using the LED, the luminescence signal strength is much reduced. To achieve a sufficiently high signal-to-noise-ratio (SNR), the illumination time is largely extended from 5 ns to 800 μs, as depicted in the lower part of **Figure 2 right**. Besides, the exposure of frame 1 is shifted ahead to fully coincide with the photoexcitation, while frame 2 covers the whole emission phase of the photoluminescence. Furthermore, the generally used high-speed camera is replaced with a low-speed camera with more sensitive sCMOS sensor and higher bit depth. With these measures, the SNR of the raw image captured with the LED is comparable with which captured with the laser.
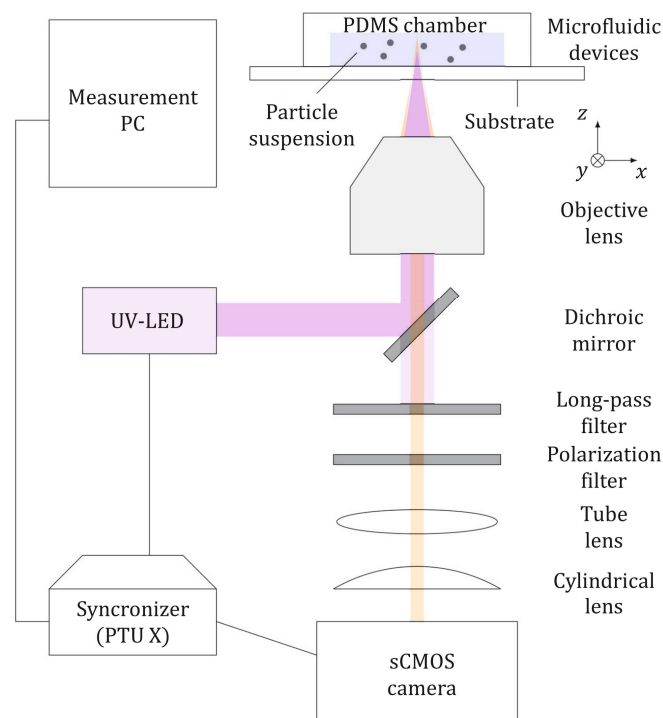
Figure 1: A schematic of the measurement setup.
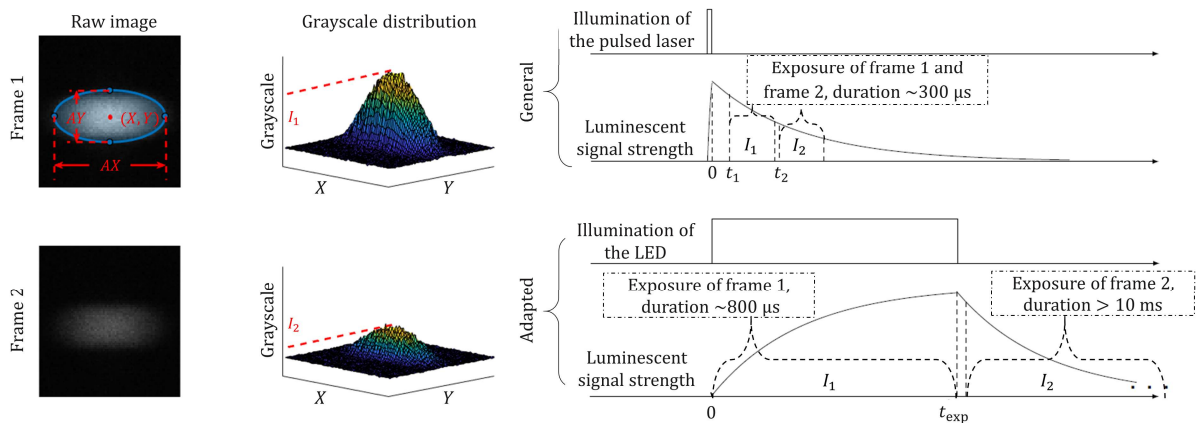
Figure 2: The raw image and grayscale distribution of a typical particle image on frame 1 and frame 2, showing how its 3D coordinates and temperature can be estimated **(left)**, and a comparison of the general timing schedule and the adapted one **(right)**.

Calibration

As mentioned in the last section, a calibration is necessary for the association of the temperature T and the intensity ratio R. It was done with particles located at the middle of the measurement depth. The set temperature T_s was controlled by a Peltier element and measured by a PT100 sensor. As depicted in **Figure 3 left**, during the calibration we dynamically varied the set temperature T_s as a sinusoidal signal, represented by the yellow curve. For every double-frame image, the intensity ratios were determined for all particle images within the field of view. They were averaged afterwards, yielding a spatial averaged intensity ratio $\overline{R}$, which is depicted in the figure as the blue curve. With such arrangement, an exponential decay of the intensity ratio caused by photobleaching can be found. After applying a correction, the orange curve and the yellow one seemed to be exactly in opposite phase as the behavior of the intensity ratio is contrarily to the temperature. With this approach, when a certain batch of particles was exposed multiple times, the bias on the measurement caused by photobleaching can be corrected. This is necessary as in applications with stagnant fluid particles are illuminated several times.

In **Figure 3 right**, the spatial averaged intensity ratio $\overline{R}$ is plotted against the set temperature T_s (blue circles). Data collected in eight temperature ramping/cooling cycles overlap well with each other, showing a good repeatability of the calibration measurement. This data was fitted according to an Arrhenius type of function (Peng et al. 2010) represented by the blue curve in the figure, which were used as the calibration curve for the real measurements. The deviation between the set temperature and the measured value is plotted as the orange cross markers. Its mean value close to $0\,°\mathrm{C}$ shows that the measurement is almost unbiased. Its standard deviation of $0.45\,°\mathrm{C}$ implies that the temperature can be very precisely measured if all the particles are in the same height. Repeated calibration measurements under different conditions showed that the calibration curve changes with the type of fluid, the type of glass or substrate at the bottom of the microfluidic chamber and the magnification of objective lens.

For the calibration of the location measurement, particles settled on the substrate were used as targets. The substrate was traversed in all three directions with well-known distances. With the corresponding displacement in the lateral plane, scaling factors in x- and y-direction were estimated. With the different AX and AY of the particle images in different z-location, a calibration curve was determined following the approach elaborated in Cierpka et al. (2011).
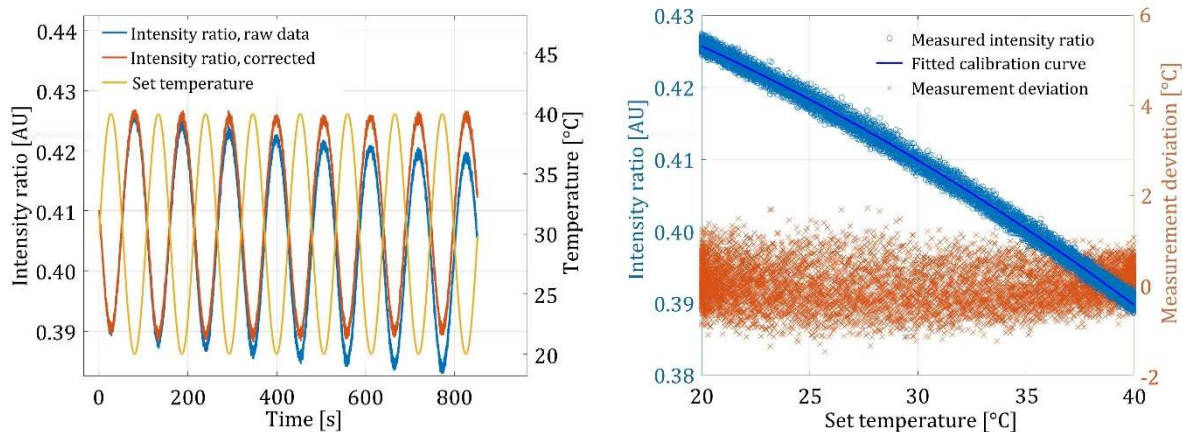
Figure 3: Intensity ratio as a function of time before and after correction and the dynamically varying set temperatures **(left)**, and experimental data, the calibration curve and the deviation on temperature measurement **(right)**. Each marker represents the corresponding spatial averaged value.

Measurement uncertainties

For the combined measurement, one important source of the measurement errors is the dependence of the measured quantities on each other. The measurements of all the quantities are based on the features of the particle image and there might be correlations between them. Therefore, it is necessary to check the independence of these measurements. For this purpose, we fixed one of the measured quantities, varied the others and checked the uncertainty of the measurement. With such analysis, we found that the measurements of x- and y-coordinates are very stable against the varying z-locations and temperature. With the current setup, the measurement uncertainties (one times of standard deviation, same for below) are lower than $0.2\ \mu m$. The measurement of z-coordinate is stable against the varying lateral locations. In some cases, the change of temperature can cause thermal expansion and alter the measured value of z. However, the well-known and linear behavior between the thermal expansion and the temperature can be corrected. After the correction, the measurement uncertainty of the z-coordinate is $1.1\ \mu m$. The largest deviation comes from the temperature measurement. A certain dependence on the lateral location was found, which might be caused by the imperfection of the optical system and can be corrected by a second-order polynomial. A slight under-estimation of the temperature was observed when particles are close to the upper- and lower-limit of the measurement depth. However, the measurement is very robust in the middle range of the measurement depth. Therefore, we shrank down the measurement volume. In the reduced measurement volume, the temperature of individual particles can be measured with a very low uncertainty of around $1°C$.

Another source of error came from the largely extended illumination and exposure time. Consider on the image plane, during the exposure of frame 1, the tracer particle moves for a certain distance, such movement can cause errors for the estimation of AX and AY and therefor affect the measurement of z. It can also cause errors for the estimation of intensity and therefore affect the temperature measurement. However, with the current setup, when we are measuring a relatively low velocity, the error is low. One pixel of the movement along the lateral plane can only cause a largest error of one pixel in x, y, $0.5\ \mu m$ in z, and negligible in T. Since all the above-mentioned errors are systematic and apply on both frames in a similar way, they have only minor influence on the uncertainty of the velocity measurement.

A demonstrative measurement on an acoustic tweezer

The new concept was finally applied to the aforementioned acoustic tweezer device. Tracer particles were suspended in a glycerol-water mixture and introduced into the microfluidic chamber. After several minutes of waiting time, particles were sedimented on the substrate of the acoustic tweezer. Before turning on the acoustic tweezer, a measurement was conducted following the conventional approach using an Nd:YAG and a high-speed CMOS camera, in a repetition rate of $25\,Hz$. As shown in **Figure 4 left**, a significant temperature increase up to $2°C$ was observed within $10\,s$. Changing the setup to the adapted one with the LED and the sCMOS camera, the spatial averaged temperature was constant over time.

Furthermore, with the operation of the acoustic tweezer, the particle movement and the temperature increase were measured simultaneously. In **Figure 4 right**, the measured temperature and the z-coordinate of an exemplary particle are plotted together against time. In this figure, one can see that this particle was moved by the acoustic tweezer and then trapped at a certain height. Meanwhile, its temperature was also increased during the operation of the acoustic tweezer. With the exclusion of the light-source induced heating, one can attribute such an increase of temperature to the operation of the acoustic tweezer. For further details about the entire experiments, results and conclusions that can be drawn for the use of SAW tweezer in biological applications, we refer to Deng et al. (2021) and Weser et al. (2022).
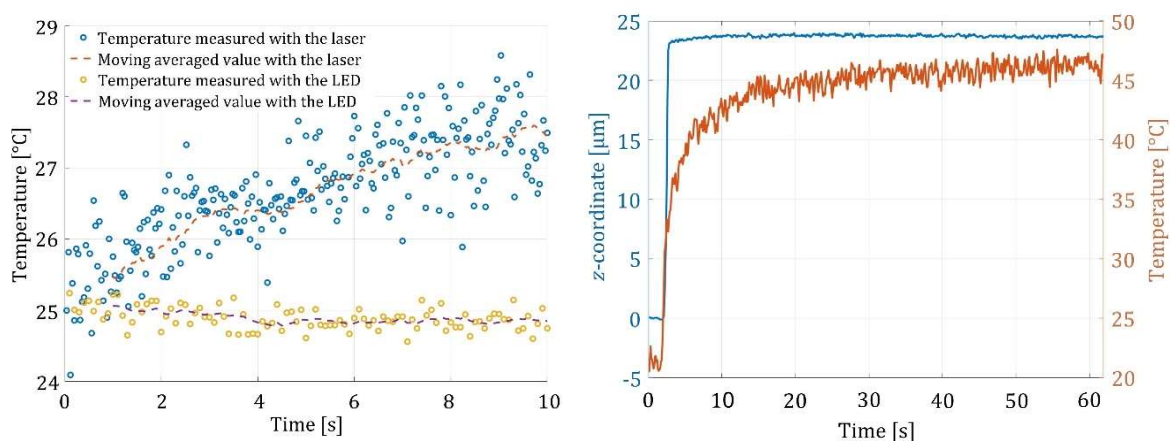
Figure 4: Measured spatial averaged temperature with the laser and with the LED as light source **(left)**, and the z-coordinate and temperature of an exemplary particle manipulated by the acoustic tweezer **(right)**.

Discussion and Summary

In this proceeding, we reported a fundamental adaptation on the conventional image-based simultaneous velocity and temperature measurement method, the astigmatism particle tracking velocimetry combined with luminescence lifetime imaging. With the replacement of the commonly used high-energetic pulsed laser with a low-power LED, additional heating caused by the light-sources was avoided. To compensate for the reduced power of the LED, the illumination and exposure time is largely extended and a more sensitive sCMOS camera is used, such that a sufficiently high signal-to-noise ratio is achieved. Furthermore, a temperature calibration with dynamically varying set temperature is proposed, with which the bias caused by photobleaching can be corrected. In addition, the uncertainties of the measurement on different quantities are strictly examined. With the current setup, under a complex measuring condition of varying locations and temperature, the measurement uncertainties on the x- and y-coordi-

nates, the z-coordinate and the temperature T are lower than $0.2\ \mu m$, $1.1\ \mu m$ and $1°C$, respectively. In addition, the measurement errors caused by the movement of tracer particles during the long illumination time are found to be quite limited when the measured velocity is low.

The technique was examined here on a microfluidic system using only one camera. In general, for other systems where temperatures are of interests and more than one camera is available, measurement techniques based on thermochromic liquid crystals (TLC) is also applicable (Moller et al. 2021). Besides, in the case of higher volume flow rates, the standard technique of APTV and LLI proposed by Massing et al. (2018) is applicable. Compared to these methods, with the current system, the measurable range of the velocity was reduced. However, many advantages are gained, including the lower cost on the devices, comparable measurement uncertainties and most important, no heating caused the light source. These features make the adapted measurement method especially suitable for the measurements done in small volume of almost stagnant fluid.

Acknowledgements

References

Cierpka, C., Lütke, B., Kähler, C. J., 2013: Higher order multi-frame particle tracking velocimetry. Exp. in Fluids, 54:1-12

Cierpka, C., Kähler, C. J., 2012: Particle imaging techniques for volumetric three-component (3D3C) velocity measurements in microfluidics. Journal of visualization, 15:1-31

Cierpka, C., Rossi, M., Segura, R., Kähler, C. J., 2011: On the calibration of astigmatism particle tracking velocimetry for microflows. Meas. Sci. Technol., 22:015401

Cierpka, C., Segura, R., Hain, R., Kähler, C. J., 2010: A simple single camera 3C3D velocity measurement technique without errors due to depth of correlation and spatial averaging for microfluidics. Meas. Sci. Technol., 21:045401

Collins, D. J., Morahan, B., Garcia-Bustos, J., Doerig, C., Plebanski, M., Neild, A., 2015: Two dimensional single-cell patterning with one cell per well driven by surface acoustic waves, Nat. Commun., 6:8686

Das, P., Snider, A., Bhethanabotla, V., 2019: Acoustothermal heating in surface acoustic wave driven microchannel flow, Phys. Fluids, 31:106106

Deng, Z., Kondalkar, V., Weser, R., Schmidt, H., Cierpka, C., König, J., 2021: Experimentelle Untersuchung eines SAW-Systems zur Parallelanalyse einzelner Zellen, Proceedings in 28. Fachtagung „Experimentelle Strömungsmechanik", Bremen

Massing, J., Kaden, D., Kähler, C. J., Cierpka, C., 2016: Luminescent two-color tracer particles for simultaneous velocity and temperature measurements in microfluidics. Meas. Sci. Technol., 27:115301

Massing, J., Kähler, C., Cierpka, C. J., 2018: A volumetric temperature and velocity measurement tech-nique for microfluidics based on luminescence lifetime imaging, Exp. in Fluids 59:163

Moller, S., Resagk C., Cierpka C, 2021: Long-time experimental investigation of turbulent superstructures in Rayleigh–Bénard convection by noninvasive simultaneous measurements of temperature and velocity fields, Exp. in Fluids 62:1-18.

Peng, H., Stich, M. I., Yu, J., Sun, L.-n., Fischer, L. H., Wolfbeis, O. S., 2010: Luminescent europium (iii) nanoparticles for sensing and imaging of temperature in the physiological range, Adv. Mater., 22:716-719

Weser, R., Deng, Z., Kondalkar, V., Darinskii, A. N., Cierpka, C., Schmidt, H, König, J., 2022: Three-dimensional heating and patterning dynamics of particles in microscale acoustic tweezers, under review in Lab Chip